

Panel Flutter Detection and Control Using Eigenvector Orientation and Piezoelectric Layers

Nebojsa Sebastijanovic*

University of California, Santa Barbara, Santa Barbara, California 93106

Tianwei Ma[†]

University of Hawaii at Manoa, Honolulu, Hawaii 96822

and

Henry T. Y. Yang[‡]

University of California, Santa Barbara, Santa Barbara, California 93106

DOI: 10.2514/1.22665

A basic eigenvector orientation approach has been used to evaluate the possibility of controlling the onset of panel flutter using a simple flat panel (wide beam) as an illustrative example. The use of the eigenvector orientation method for prediction of the flutter boundary (indicated by a gradual loss of orthogonality between two eigenvectors) was developed in a previous study and can thus provide a lead time for possible flutter control. As a first step, piezoelectric layers are assumed to be bonded to the top and bottom surfaces of the panel in order to provide counterbending moments at joints between elements. The standard linear quadratic control theory is used for controller design and full state feedback is considered for simplicity. The controllers are designed to restabilize the system at the onset of flutter; as a result, flutter occurrence can be offset to a higher flutter speed. To illustrate the applicability and effectiveness of the developed method, several simple wide-beam examples are studied and presented. The effects of control moment locations are studied so as to fulfill the objective of adjusting the flutter speed to be within a desirable range. Potential applications of this basic method may be straightforwardly applied to plate and shell structures of laminated composites using the versatile finite element method.

I. Introduction

FLUTTER is frequently found in flexible aircraft structures that can vibrate with bending and twisting motions under the influence of aerodynamic loads. Dynamic instability develops once the structure begins to vibrate in a periodic manner and dynamic airloads cause the amplitude to grow. Flutter has been one of the most destructive causes of failure of concern in the design of aircraft, missiles, and various flight vehicles [1–4]. Flutter has even been observed in civil structures such as suspension bridges [5–7] and natural draught hyperbolic paraboloid cooling towers and tall chimneys [8–11]. One of the first solutions was to increase the stiffness of the structure but that was neither always possible nor always feasible due to weight considerations or other limitations such as performance requirements. Flutter is also affected by the mass distribution of a structure as much as its stiffness. Mass balancing of aircraft components has become an important task in aircraft design to prevent flutter. However, as maximum flight velocities of aircraft continue to increase, there is a need for a more effective method of flutter prediction and control, especially at transonic and supersonic speeds. In recent years, reports on accidents where flutter was the cause of the crash continue. The better known, and also more significant, crashes during supersonic flights include Taiwan's IDF fighter in 1992, a prototype of an American fighter F-22 also in 1992, and the U.S. Air Force F-117 in 1997 [12].

Conventional techniques using mass balancing and local stiffening are still currently used in smaller airplanes to prevent flutter, but may not be as desirable for modern aircraft because these methods may add weight to the complex structure and are not necessarily guaranteed to work. Weight reduction is considered one of the major design objectives in modern aircraft design. Weight reduction, however, can reduce structural stiffness and could therefore lower the critical flutter speed. There have also been attempts to introduce a flutter suppression system that would offset flutter occurrence to a higher-pressure condition and expand the flight envelope [13–18].

Flutter analysis has been included in many textbooks on aeroelasticity; a few of particular interest are by Bisplinghoff and Ashley [1], and Dowell [2]. One popular approach to treat the panel flutter problem is to use finite elements in the form of thin wide beams, plates, and shells to take advantage of their versatility in geometric and material modeling. Some of the earliest demonstrations using finite elements to solve the panel flutter problem were by Olson for wide-beam elements [19] and rectangular plate elements [20], and later by Yang et al. for flat panels [21–23]. Using the concept of formulating an aerodynamic matrix in addition to the stiffness and mass matrices of a finite element, Olson [19,20] was able to solve the panel flutter problem using the definition that flutter occurs when two modes coalesce. In a more recent work by Afolabi, Pidaparti, and Yang [24], an alternative approach based on the eigenvector orientation was developed to detect the onset of flutter. Because the response time is critical in the flutter control process and design, generating a lead time is important and could be established by tracking the eigenvectors and the angle between them as it gradually approaches zero. This lead time may provide more room for a study of more effective control and prevention of flutter that flight vehicles with plate and shell structures might experience.

In this study, piezoelectric layers are used as actuators that provide counterbending moments at joints between elements. Application of piezoelectric sensors and actuators has become of interest in the fields of the so-called smart structures and structural vibration control over the past decade. There are many papers dealing with the issue of structural vibration control using piezoelectric actuators. For example, Liu and Yang [14] presented a piezoelectric actuator that is

Received 24 January 2006; revision received 30 July 2006; accepted for publication 5 October 2006. Copyright © 2006 by the American Institute of Aeronautics and Astronautics, Inc. All rights reserved. Copies of this paper may be made for personal or internal use, on condition that the copier pay the \$10.00 per-copy fee to the Copyright Clearance Center, Inc., 222 Rosewood Drive, Danvers, MA 01923; include the code \$10.00 in correspondence with the CCC.

*Research Assistant, Department of Mechanical and Environmental Engineering. Student Member AIAA.

[†]Assistant Professor, Department of Civil and Environmental Engineering. Member AIAA.

[‡]Professor and Chancellor, Department of Mechanical and Environmental Engineering. Fellow AIAA.

effective in the vibration control of a slewing beam system, whereas Baz, Poh, and Fedor [13], presented a control algorithm for a cantilever beam. Forster and Yang [18] used piezoelectric actuators to control supersonic flutter of wing boxes. Piezoceramic layers were used both as sensors and actuators in a study by Hanagud, Obal, and Calise [25].

This paper proposes the use of the eigenvector orientation approach in conjunction with a control algorithm to circumvent the onset of flutter. The finite element formulation, the controller design, and the solution procedures are developed. To illustrate the applicability and effectiveness of the developed method, several simple wide-beam examples using piezoelectric layers as actuators are studied and presented.

II. Finite Element Formulation

A simple four degrees of freedom wide-beam element (with a transverse deflection and a bending rotation at each of the two joints) was used to model the current example of a wide-beam type of panel. In the current illustrative examples, four elements were used to model the panel as shown in Fig. 1.

Control bending moments are assumed to be applied through the use of piezoelectric layers placed on the top and the bottom layers of the beam. This is also shown in Fig. 1. The thickness of these piezoelectric layers was assumed to be small as compared with the depth of the beam so that the structural changes due to these layers can be considered negligible [25,26].

Piezoelectric materials have a property that, when subjected to a mechanical strain, a voltage proportional to the strain is produced. On the other hand, when applying a voltage to the piezoelectric element, they produce mechanical strains in the material. The linear piezoelectric constitutive equations for piezoelectric elements can be written as [27]

$$\sigma = c^E \varepsilon - e^T E \quad D = e \varepsilon + \epsilon^S E \quad (1)$$

where c^E is the elastic stiffness matrix, E is the electric field vector, D is the electric displacement vector, ϵ^S is the dielectric constant matrix, and e is the piezo stress/charge constant.

Bending moments can be calculated using the stress-strain relationship for the isotropic piezoelectric layer. Thus, piezoelectric materials can be used as actuators to apply control moments to restabilize the system. Piezoelectric layers are independently applied to the top and bottom part of each beam element. This allows for different combinations (in both magnitude and direction) of control bending moments to be applied; because each element has a separate piezoelectric layer, depending on the voltage applied, each element can experience a positively or negatively defined bending moment by having the top layer in compression and the bottom layer in tension, or vice versa.

In this study, only three simple examples are considered for illustrative purpose. The three cases considered are shown in Fig. 2a. Controllers are designed to modify the system stiffness matrix by assuming that control bending moments are applied on all four elements, on the two interior elements, or on the two end elements. Control bending moments are assumed to be created by the use of

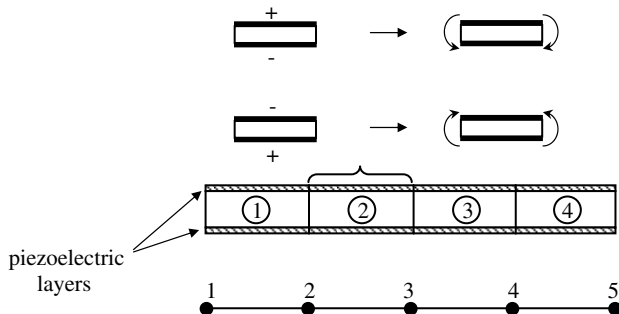


Fig. 1 Beam configuration, beam element, and moments created by piezoelectric layers.

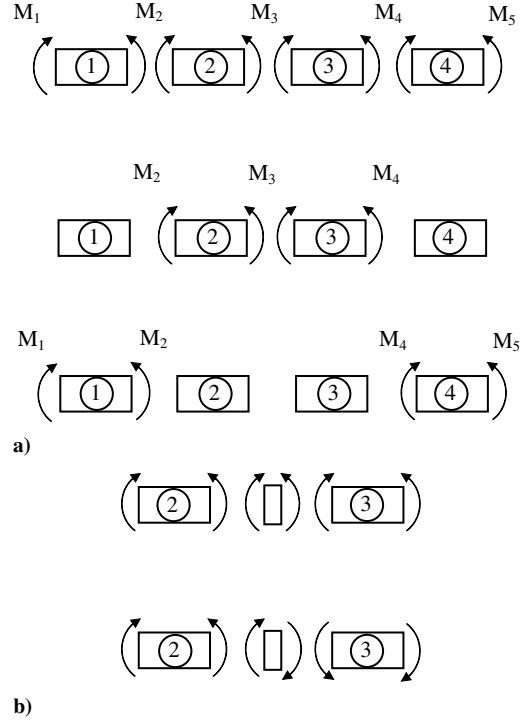


Fig. 2 a) Control moment combinations, and b) equivalent external moments created at a joint.

piezoelectric layers. These bending moments are equivalent to an external moment applied at a joint between the two elements, as shown in Fig. 2b. Depending on the direction and magnitude of the control bending moment at both adjacent elements, the resulting moment (equivalent to an external moment) at a joint can be created and adjusted.

The equation of motion for an actively controlled finite element beam subjected to aerodynamic loads may be written as [28,29]

$$[M][\ddot{Q}_i] + [C][\dot{Q}_i] + ([K] + [A_e] + [K_1] + [K_2]) - [K_{w\varphi}][K_{\varphi\varphi}]^{-1}[K_{w\varphi}][Q_i] = [K_{w\varphi}]V_a \quad (2)$$

where $[M]$, $[C]$, $[K]$ are the mass, damping, and stiffness matrices, $[A_e]$ is the aerodynamic matrix, $[K_1]$ and $[K_2]$ are the nonlinear stiffness matrices, $[K_{w\varphi}]$ is the elastic-electric coupling stiffness matrix, $[K_{\varphi\varphi}]$ is the dielectric stiffness matrix, $[Q_i]$ are the vectors for joint displacements, and V_a is the applied voltage. It should be noted that because angles between the eigenvectors (natural modes) are used in this study to determine the onset of flutter, the damping term in the preceding equation is not used when calculating the eigenvectors.

The aeroelastic system of equations for the structure is obtained by assembling the element matrices, which can be symbolized by capital letters as shown in the preceding equation. The element stiffness and mass matrix formulation can be found in [19], whereas the aerodynamic matrix (which accounts for the aerodynamic flows) formulation can be derived from the principle of virtual work, and can be found, for example, in [20,21]. A computer program has been developed with the capability to predict the onset of coupled mode flutter based on the gradual loss of orthogonality of eigenvectors for a general flat panel (wide beam) with arbitrary boundary conditions.

As a first step, this study is limited to the range of airspeed for which linear aerodynamic modeling is admissible. Analysis of nonlinear aerodynamics is not within the scope of the current investigation. Neglecting the nonlinear matrices $[K_1]$ and $[K_2]$, Eq. (2) can also be written as

$$[M][\ddot{Q}_i] + [C][\dot{Q}_i] + ([K] + A[K_a])[Q_i] = [u] \quad (3)$$

where $[u] = [K_{w\varphi}][K_{\varphi\varphi}]^{-1}[K_{w\varphi}][Q_i] + [K_{w\varphi}]V_a$. The applied voltage can be expressed as

$$V_a = [K_{w\varphi}]^{-1}([u] - [K_{w\varphi}][K_{\varphi\varphi}]^{-1}[K_{w\varphi}][Q_i]) \quad (4)$$

In this study, the control moments $[u]$ were used in the controller design instead of V_a for simplicity.

Assuming a first order, high Mach number M_∞ approximation to the linear piston theory, the aerodynamic pressure acting on a surface is given in [20] as

$$p = \frac{2q_f}{\sqrt{(M_\infty^2 - 1)}} \left(\frac{\partial}{\partial x} + \frac{1}{U} \frac{M_\infty^2 - 2}{M_\infty^2 - 1} \frac{\partial}{\partial t} \right) w \quad (5)$$

where q_f is the freestream dynamic pressure, M_∞ is the Mach number, U is the flow velocity, and with the nondimensional aerodynamic pressure parameter defined as

$$A = \frac{2q_f L^3}{D \sqrt{(M_\infty^2 - 1)}} \quad (6)$$

where L is the length of the element and D is the bending rigidity.

The angle between two eigenvectors is computed from their scalar product. For two real vectors, the angle is the arc cosine

$$\theta = \cos^{-1} \left(\frac{v_1 \cdot v_2}{\|v_1\| \|v_2\|} \right) \quad (7)$$

The angle between two complex vectors is computed by replacing one of the vectors by its complex conjugate before computing their scalar product, so that

$$\theta = \cos^{-1} \left(\frac{\bar{v}_1 \cdot v_2}{\|\bar{v}_1\| \|v_2\|} \right) \quad (8)$$

where an overbar indicates complex conjugation.

III. Controller Design

The controller used in this paper is designed using the linear quadratic regulator theory [30]. It is designed to restabilize the system by modifying the system stiffness matrix. Each controller is based on the structural model with a specific aerodynamic pressure parameter, indicated as A_c . Several different actuator locations have been evaluated as well. The state-space representation of Eq. (3) can be written as

$$\{\dot{x}\} = [F] \cdot \{x\} + [B] \cdot \{u\} \quad (9)$$

where

$$\{x\} = [Q_i \quad \dot{Q}_i]^T, \quad [F] = \begin{bmatrix} 0 & I \\ -M^{-1} \cdot K & 0 \end{bmatrix}$$

and $[B]$ can be determined according to the actuator configuration, for example,

$$[B] = [0 \quad I]^T$$

when all four elements are controlled.

The control law is found by minimizing the following quadratic cost function

$$\{J\} = \int_{t_0}^{\infty} (\{x\}^T [Q] \{x\} + \{u\}^T [R] \{u\}) dt \quad (10)$$

where $[Q]$ and $[R]$ are the weighting matrices for control effects and control efforts (in this study, $[Q] = q^*[I]$ and $[R] = r^*[I]$, where q and r are constants).

The linear feedback control force vector can be written as

$$\{u\} = -[R]^{-1}[B]^T[P]\{x\} = [G]\{x\} \quad (11)$$

where $[P]$ is the so-called Riccati matrix and can be obtained by

solving the algebraic Riccati equation

$$[F]^T[P] + [P][F] - [P][B][R]^{-1}[B]^T[P] + [Q] = 0 \quad (12)$$

Using the feedback control in Eq. (11), the system matrix $[F]$ is modified to be $[F] + [\Delta F]$, where $[\Delta F]$ can be written as

$$[\Delta F] = [B][G] = \begin{bmatrix} 0 \\ 1 \end{bmatrix} [G_1 \quad G_2] = \begin{bmatrix} 0 & 0 \\ G_1 & G_2 \end{bmatrix} \quad (13)$$

Therefore, the stiffness coefficient change induced by the feedback control can be written as

$$[\Delta K] = [M][G_1] \quad (14)$$

This change in the stiffness matrix from Eq. (14) represents the effect that would be created by applied control moments using piezoelectric layers and is added to Eq. (3). Therefore, by using the structural responses, the controller is able to restabilize the system by modifying the system stiffness matrix. It should be noted that the actual applied voltage needed to achieve this change in the stiffness matrix can be calculated using Eq. (4).

IV. Numerical Simulations

A set of examples has been analyzed to find combinations of control parameters that would result in offsetting flutter to a higher speed. These examples included using different locations for the application of control bending moments as well as using various controllers. Different controllers were obtained by fixing the weighting matrix R while varying the weighting matrix Q in the controller design procedure.

In each simulation, a simply supported isotropic plate in the form of a wide beam with a width of unity, length l , and thickness t in. was analyzed. The material properties for this isotropic aluminum beam were assumed to be modulus of elasticity $E = 10$ Mpsi, Poisson's ratio $\nu = 0.3$, and mass density $\rho = 0.025 \text{ lb} \cdot \text{s}^2/\text{in}^4$. The piezoelectric layer thickness was assumed to be 0.0005 m and the material properties were assumed to be modulus of elasticity $E = 66 \text{ GPa}$, Poisson's ratio $\nu = 0.31$, mass density $\rho = 7800 \text{ kg/m}^3$, piezoelectric coefficient $d_{31} = -190 \times 10^{-12} \text{ m/V}$, $h_{31} = -1.622 \times 10^9 \text{ N/C}$, and maximum electric field $5 \times 10^5 \text{ V/m}$, similar to those used in [28]. For the purpose of simplicity in presenting the present illustrative examples, all beams were modeled first with four elements and then with six and eight elements. The eigenvector orientation method was used to plot all results and evaluate the effectiveness of different control parameter combinations. The aerodynamic pressure parameter defined in Eq. (4) is used in all figures to indicate the flutter speed. The value of the aerodynamic pressure parameter indicated by A_c was used in the controller design to define the structural model.

As a first step, both the present eigenvector orientation method and the coalescence of eigenvalues method were used to analyze this example. As shown in Fig. 3a, flutter occurs as the lowest two eigenvalues coalesce around a critical value of aerodynamic pressure parameter at $A = 343$. This corresponds to the flutter condition when the angle between the two eigenvectors drops to zero and yield the same value at $A = 343$ as shown in Fig. 3b.

In this study, each controller is designed based on a model with a specific aerodynamic pressure parameter, which is indicated as A_c . Controllers are designed to determine the necessary change in the stiffness matrix $[\Delta K]$ to stabilize the system and offset flutter to a higher pressure. This $[\Delta K]$ can then be used to determine external moments that need to be applied at joints. External moments are assumed to be applied through the use of piezoelectric layers. The magnitude of the necessary control bending moments can be calculated for the particular application by using the following equation:

$$[F_1 \quad M_1 \quad F_2 \quad M_2 \quad F_3 \quad M_3 \quad F_4 \quad M_4 \quad F_5 \quad M_5]^T = [\Delta K][Q_i] \quad (15)$$

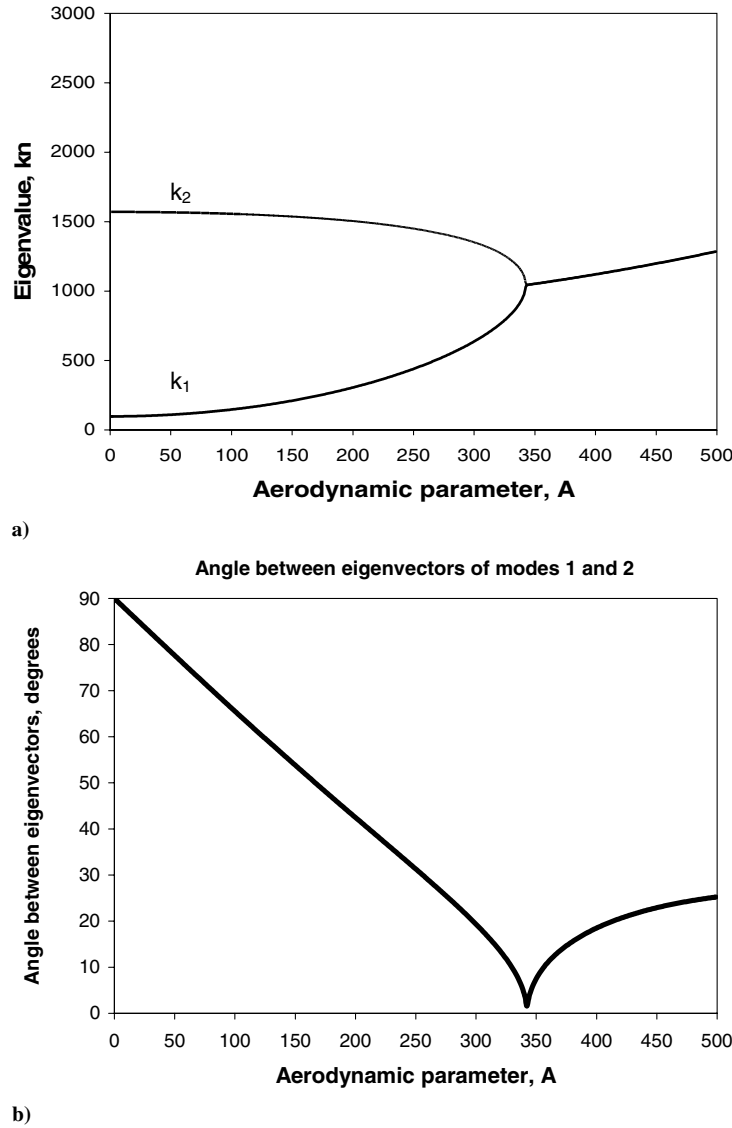


Fig. 3 a) Coalescence of eigenvalues, and b) eigenvector orientation method.

where F_i , M_i = force and moment at joint i , and $[Q_i]$ = displacements and rotations

It should be noted that $[\Delta K]$ has nonzero terms only for those rows that relate moments and rotations.

A. Case 1: Applying Control Moments on all Four Elements

Assuming that the control bending moments are applied on all four elements, flutter speed can be both decreased and increased depending on the controller design. This concept is illustrated in Fig. 4 where different combinations of control parameters q and A_c were used to obtain eight flutter speeds varying from $A = 50$ to $A = 650$ including the uncontrolled case of $A = 343$.

For simplicity of presentation of this example, all flutter speeds, control parameters q and A_c are listed in Table 1. It is noticed that for $A_c = 0$, flutter speed increases as the control parameter q decreases. However, by using $A_c = 0$, flutter speed cannot be increased above $A = 343$ (uncontrolled case). Once the control parameter A_c is increased to 300 or 400, flutter speeds can be increased above $A = 343$. In both cases, flutter speed increases as the control parameter q increases. It should be noted that this is opposite of that observed for the case when $A_c = 0$.

It is of interest to look into the mode shapes associated with this case of flutter analysis and control. The eigenvalues for the two lowest modes for various values of A are plotted in Fig. 5 for a specific case with $q = 0.0001$ and $A_c = 400$. It is seen that the two

lowest eigenvalues coalesce and become complex at $A = 350$, indicating the onset of flutter. The corresponding mode shapes for this specific case are shown for five specific values of A from zero to 600 in Table 2.

For the uncontrolled case, it is seen that the two lowest modes are distinct at $A = 0$ and 200, indicating stability. However, the two lowest modes become similar at $A = 350$, and also at $A = 500$ and 600, indicating a flutter condition.

When the controller is applied, it is seen that the two mode shapes became distinct at $A = 350$, as well as in all other A values as shown in Table 2. Of course, in cases when $A = 0$ and 200, flutter does not occur and application of the controller does not alter the distinction of the two lowest modes.

B. Case 2: Applying Control Moments on the Two Interior Elements

If the same procedure is repeated for the case when the control bending moments are assumed to be applied only on the two interior elements (elements 2 and 3 in Fig. 1), flutter speed can again be both decreased and increased depending on the controller design. This concept is illustrated in Fig. 6 where different combinations of control parameters q and A_c were used to obtain seven flutter speeds varying from $A = 100$ to $A = 500$ including the uncontrolled case of $A = 343$.

Once again, all flutter speeds, control parameters q and A_c are listed in Table 3 for simplicity. The same trends can be seen as in the

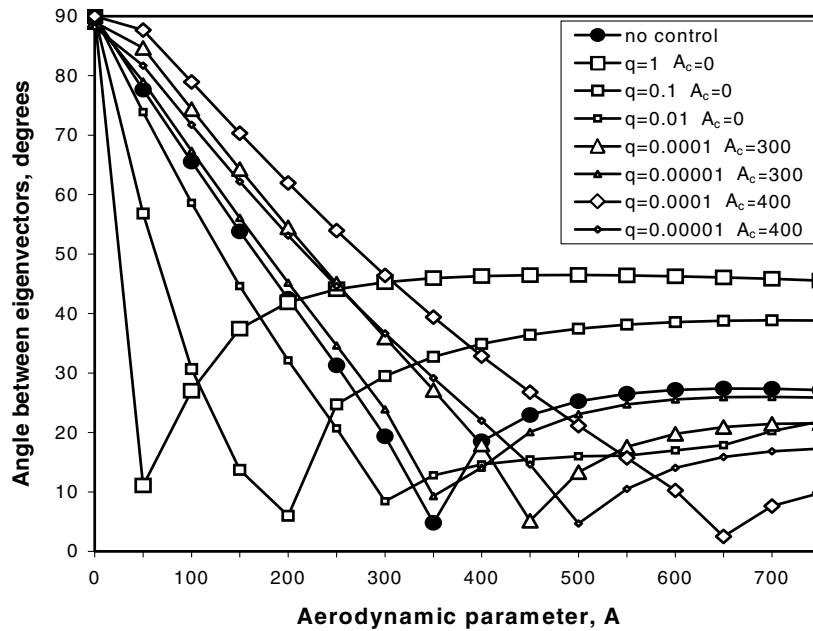


Fig. 4 Angle between modes 1 and 2 with control moments on all four elements.

case when the control moments were assumed to be applied on all four elements: for $A_c = 0$, flutter speed increases as the control parameter q decreases, whereas for $A_c = 300$ or 400 flutter speed increases as the control parameter q increases. Flutter speed can be increased above $A = 343$ only when $A_c = 300$ or 400 . For the examples studied, the major difference is that the flutter speed cannot be increased as much as in the first case when it was offset to $A = 650$. The maximum offset for this case is around $A = 500$.

The eigenvalues for the two lowest modes for various values of A are plotted in Fig. 7 for a specific case with $q = 0.0001$ and $A_c = 400$. The corresponding mode shapes for this specific case are shown for five specific values of A from zero to 450 in Table 4.

Similar to the case when the control moment is applied on all four elements, the lowest two modes change the most. For the uncontrolled case, two lowest modes become similar at $A = 350$, and also at $A = 400$ and 450 , indicating a flutter condition. When the controller is applied, it is observed that the two mode shapes are distinct at $A = 350$, as well as in all other A values above 350 as shown in Table 4. Of course, in cases when $A = 0$ and 150 , flutter does not occur and application of the controller does not alter the distinction of the two lowest modes.

C. Case 3: Applying Control Moments on the Two End Elements

Assuming that the control bending moments are only applied on the two end elements (elements 1 and 4 in Fig. 1), flutter speed can only be increased. This is illustrated in Fig. 8 where different combinations of control parameters q and A_c were used to obtain six flutter speeds varying from $A = 400$ to $A = 650$, including the uncontrolled case of $A = 343$.

Table 1 Flutter speed for different control parameters with control moments on all four elements

Control parameters		Flutter speed
A_c	q	
0	1.0	50
0	0.1	200
0	0.01	300
uncontrolled case		343
300	0.00001	350
300	0.0001	450
400	0.00001	500
400	0.0001	650

Once again, all flutter speeds, control parameters q and A_c are listed in Table 5. The same trend can be seen as in the previous two cases: for $A_c = 300$ or 400 , flutter speed increases as the control parameter q increases. Comparing this case to the previous two cases, the major difference is that the flutter speed cannot be decreased when applying a moment only on the end two elements; it can only be increased for all values of A_c . The maximum offset for this case is around $A = 650$.

The eigenvalues for the two lowest modes for various values of A are plotted in Fig. 9 for a specific case with $q = 0.00001$ and $A_c = 400$. The corresponding mode shapes for this specific case are shown for five specific values of A from zero to 450 in Table 6.

Similar to the previous two cases analyzed, the lowest two modes change the most. For the uncontrolled case, the two lowest modes become similar at $A = 350$, and also at $A = 400$ and 450 , indicating a flutter condition. When the controller is applied, it is observed that the two mode shapes are distinct at $A = 350$, as well as in all other A values above 350 as shown in Table 6. Of course, in cases when $A = 0$ and 150 , flutter does not occur and application of the controller does not alter the distinction of the two lowest modes.

V. Modeling by More Elements

Several examples have been studied using six and eight elements to model the same simply supported flat panel (wide beam) instead of four elements. As one might expect, virtually no improvement in accuracy was achieved as the uncontrolled flutter speed was the same at $A = 343$ for both six and eight element models. However, there

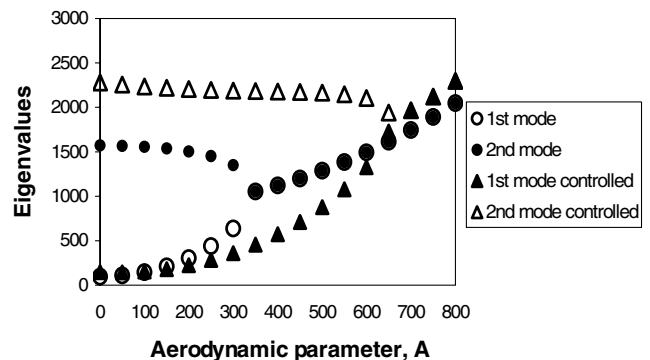






























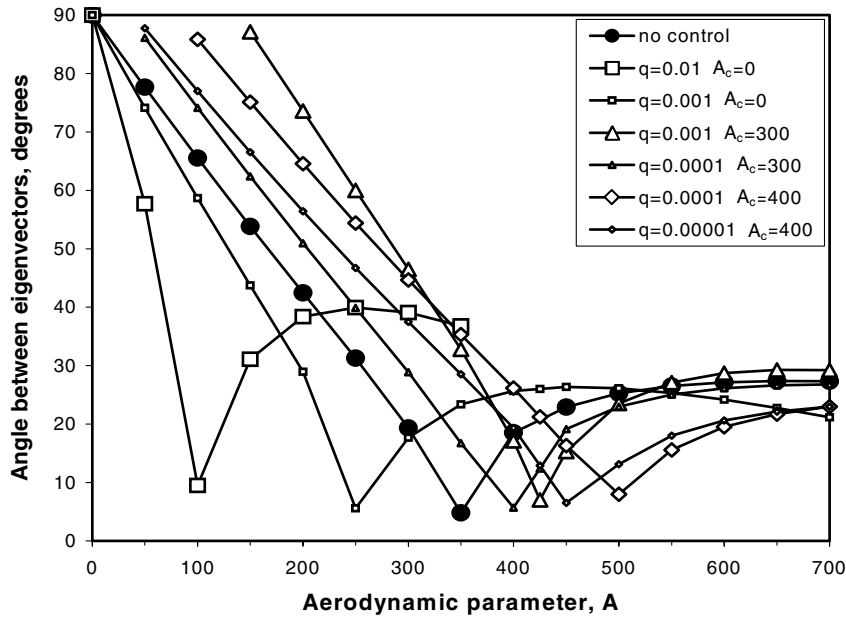


Fig. 5 Eigenvalues for $q = 0.0001$ and $A_c = 400$ with control moments on all four elements.

Table 2 Mode shapes for $q = 0.0001$ and $A_c = 400$ with control moments on all four elements

$A = 0$		$A = 200$		$A = 350$		$A = 500$		$A = 600$	
uncontrolled	controlled	uncontrolled	controlled	uncontrolled	controlled	uncontrolled	controlled	uncontrolled	controlled
									
									
									

**Fig. 6** Angle between modes 1 and 2 with control moments on two interior elements.

was a significant improvement in offsetting the flutter boundary when using six and eight elements. This seems to be due to the fact that the control moments are being applied at more joints between elements. It seems that using more elements, thus creating more external moments, can better control the mode shapes so as to more effectively keep the two coalescing modes (the two lowest modes in this case) to be distinct, i.e., to be orthogonal, mathematically speaking. For the cases considered, applying control moments on more joints between elements seems to be more effective in moving the flutter boundary to a higher speed.

All flutter speeds and control parameters q and A_c for the cases considered (four, six, and eight elements) are listed in Table 7 for

comparison. Similar trends can be seen for all three modelings used; for $A_c = 0$, flutter speed increases as the control parameter q decreases, whereas for $A_c = 300$ or 400 , flutter speed increases as the control parameter q increases. However, it is clear that the flutter speed can be increased noticeably as more elements were used in the modeling.

Flutter speed was increased to the value of $A = 900$ when using six elements and as high as $A = 1050$ when using eight elements. This is illustrated in Figs. 10 and 11 where different combinations of control parameters q and A_c were used to obtain different flutter speeds. Figure 10 shows flutter speeds varying from $A = 50$ to $A = 900$

Table 3 Flutter speed for different control parameters with control moments on two interior elements

Control parameters		Flutter speed
A_c	q	
0	0.01	100
0	0.001	250
uncontrolled case		343
300	0.00001	400
300	0.0001	425
400	0.00001	450
400	0.0001	500

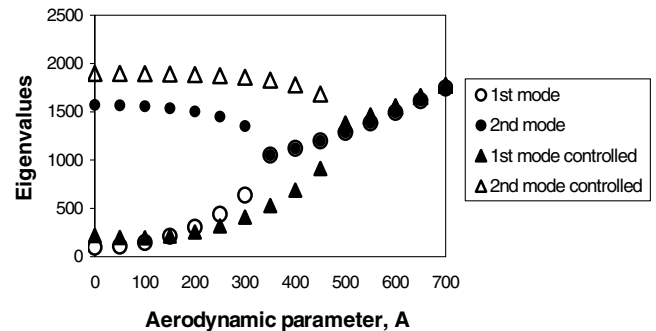















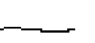

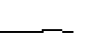

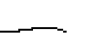





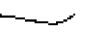




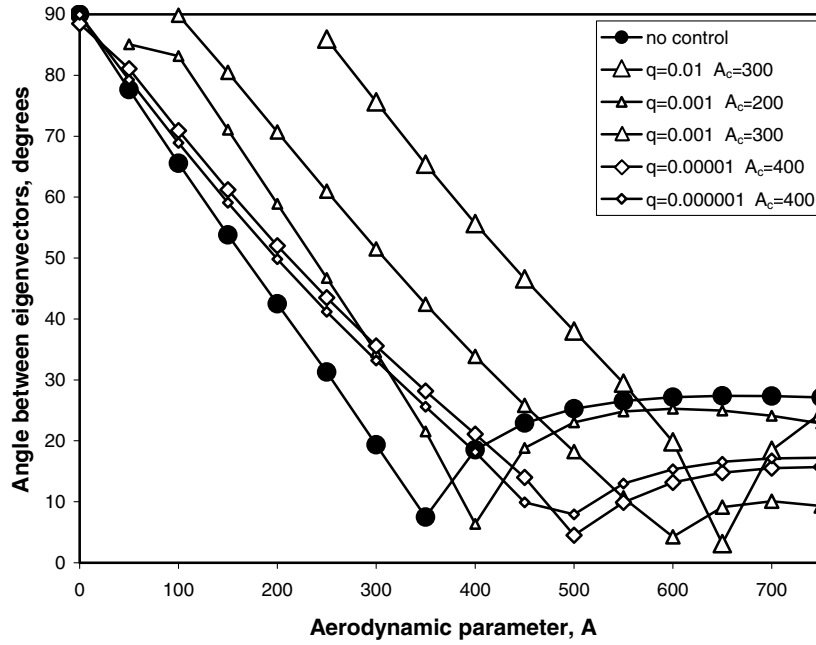
**Fig. 7** Eigenvalues for $q = 0.0001$ and $A_c = 400$ with control moments on two interior elements.

Table 4 Mode shapes for $q = 0.0001$ and $A_c = 400$ with control moments on two interior elements

$A = 0$		$A = 150$		$A = 350$		$A = 400$		$A = 450$	
uncontrolled	controlled	uncontrolled	controlled	uncontrolled	controlled	uncontrolled	controlled	uncontrolled	controlled
									
									
									

**Fig. 8** Angle between modes 1 and 2 with control moments on two end elements.**Table 5** Flutter speed for different control parameters with control moments on two end elements

Control parameters		Flutter speed
A_c	q	
uncontrolled case		343
200	0.001	400
300	0.001	600
300	0.01	650
400	0.000001	475
400	0.000001	500

when using six elements. Figure 11 shows flutter speeds varying from $A = 50$ to $A = 1050$ when using eight elements.

VI. Conclusions

A method of flutter control for a simply supported flat panel using the eigenvector orientation approach and piezoelectric layers has been developed. Several cases have been presented and the results show that the flutter occurrence can be offset to a lower or higher speed by applying control bending moments to some or all of the elements of the beam through the use of piezoelectric layers. The

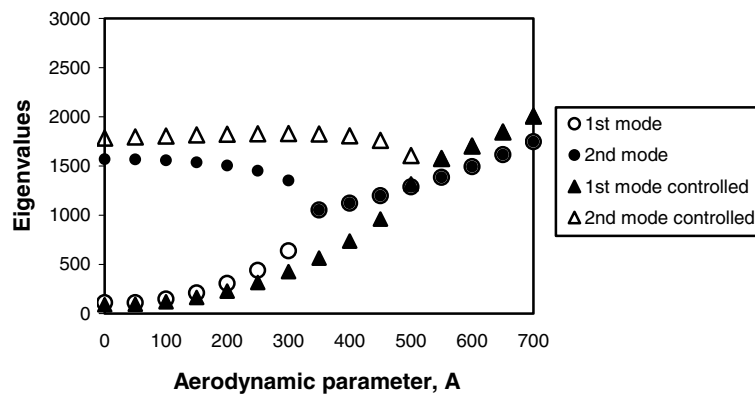
**Fig. 9** Eigenvalues for $q = 0.00001$ and $A_c = 400$ with control moments on two end elements.

Table 6 Mode shapes for $q = 0.00001$ and $A_c = 400$ with control moments on two end elements




















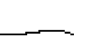





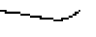




$A = 0$		$A = 150$		$A = 350$		$A = 400$		$A = 450$	
uncontrolled	controlled	uncontrolled	controlled	uncontrolled	controlled	uncontrolled	controlled	uncontrolled	controlled
									
									
									

Table 7 Flutter speed for different control parameters with control moments on two end elements

Control parameters		Flutter speed		
A_c	q	4 elements	6 elements	8 elements
0	1.0	50	50	50
0	0.1	200	150	100
0	0.01	300	300	250
uncontrolled case		343	343	343
300	0.00001	350	400	450
300	0.0001	450	850	950
400	0.00001	500	550	650
400	0.0001	650	900	1050

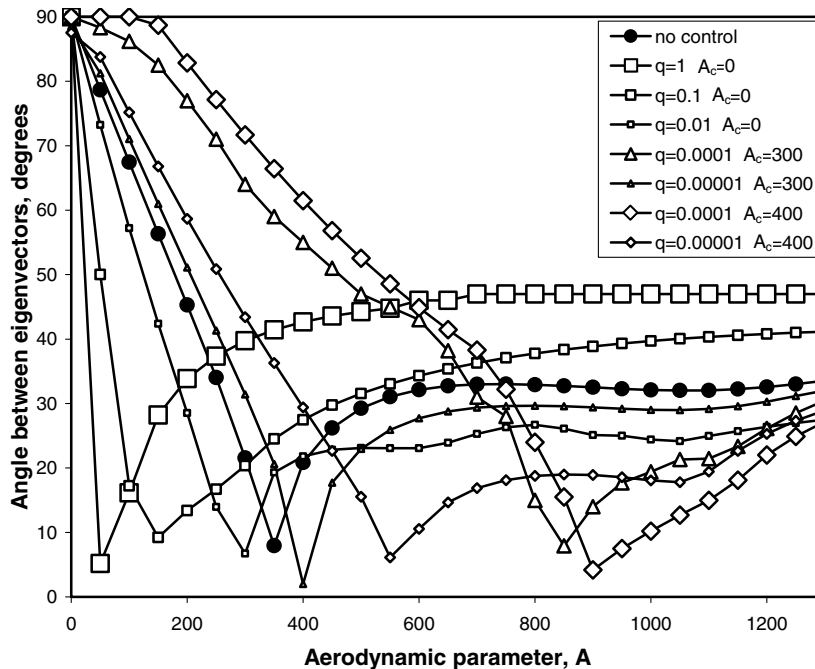
effectiveness of moving the flutter boundary depends on the number of elements, control moment locations used, and the control parameters q and A_c . In the examples studied, it is shown that for higher values of A_c , by increasing the control parameter q , the flutter speed is offset to a higher speed in all cases. However, there is a limitation as to how much the flutter boundary can be offset. After a certain point, increasing the value of the control parameter q does not seem to result in a higher flutter speed.

It was observed that when the control moments were applied on all four elements, the flutter speed was increased more than when

applying the control moment on only the two interior elements or on the two end elements. This might be due to the difference that applying the control bending moments on all four elements produces external moments at each of the five joints, whereas applying the control bending moments on two elements creates external moments only at three interior joints. It seems that applying control moments on more joints between elements can be more effective in moving the flutter boundary. This was also observed when the same flat panel was modeled with six and eight elements, respectively, and control bending moments were applied on all elements. In these two cases, it was observed that having more concentrated moments resulted in offsetting flutter to a higher speed for certain controller designs.

It should be noted that there are limits as to offsetting the flutter speed in each case. One limitation is that each controller can only achieve a certain amount of increase in the flutter speed. Another limitation is in the magnitude of moments that can be achieved using the piezoelectric layers. As shown in Eq. (11), the actual power needed from the piezoelectric layers is determined by the amplitude of the structural vibration. More realistic examples, including forced vibration, could be used to study the power limitations of the piezoelectric layers. Also, by using different controller designs, it is possible to have the higher modes participate in flutter as well. It would be of interest to study this phenomenon in the future.

It is a logical next step to use this basic concept to study flutter control using piezoelectric layers for panels with rectangular and

**Fig. 10** Angle between modes 1 and 2 with control moments on all six elements.

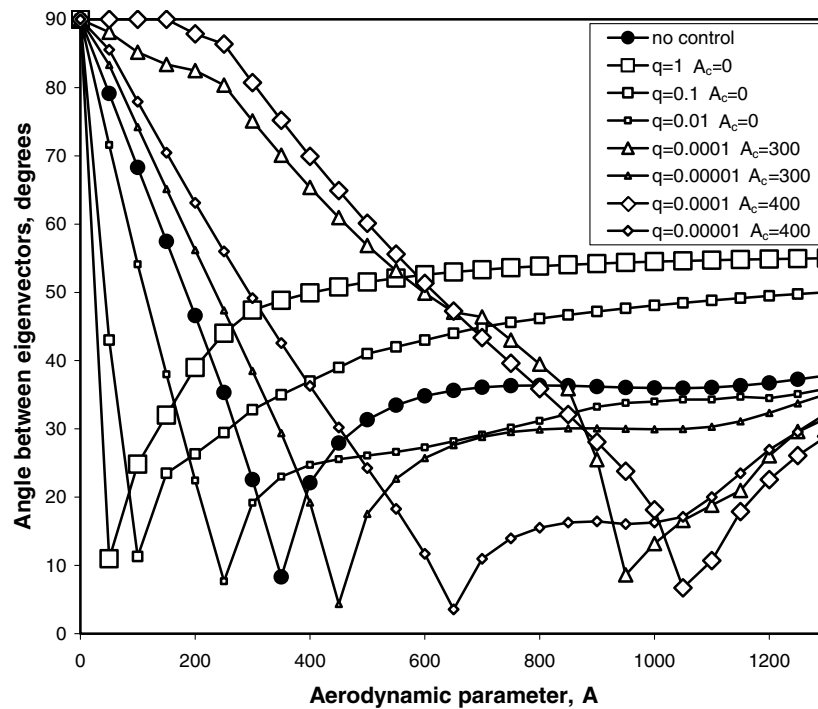


Fig. 11 Angle between modes 1 and 2 with control moments on all eight elements.

other shapes, different boundary conditions, and with various material properties, such as laminated composites. It is also a logical next step to take advantage of the lead time created by the eigenvector orientation method to develop controllers that would be capable of tracking eigenvectors before the onset of flutter.

Acknowledgments

This study was sponsored by NASA through grant NGT4-52423. The guidance of Kaja K. Gupta, Program Director, is gratefully acknowledged.

References

- [1] Bisplinghoff, R. L., and Ashley, H., *Principles of Aeroelasticity*, Dover, New York, 1962.
- [2] Dowell, E. H., *Aeroelasticity of Plates and Shells*, Noordhoff International, Leyden, The Netherlands, 1975, Chap. 2.
- [3] Garrick, E. I., and Reed, W. H., "Historical Development of Aircraft Flutter," *Journal of Aircraft*, Vol. 18, No. 1, 1981, pp. 897–912.
- [4] Friedmann, P. P., "Renaissance of Aeroelasticity and its Future," *Journal of Aircraft*, Vol. 36, No. 1, 1999, pp. 105–121.
- [5] Farquharson, F. B., Smith, F. C., and Vincent, G. S., "Aerodynamic Stability of Suspension Bridges," *Bulletin of the Structural Research Laboratory*, Pts. 1–5, Univ. of Washington, Seattle, WA, 1949–1954.
- [6] Sabzevari, A., and Scanlan, R. H., "Aerodynamic Instability of Suspension Bridges," *Journal of Engineering Mechanics*, Vol. 94, No. EM2, Proc. Paper 5889, Apr. 1968, pp. 489–519.
- [7] Beliveau, J. G., Vaicaitis, R., and Shinozuka, M., "Motion of Suspension Bridge Subject to Wind Loads," *Journal of the Structural Division*, Vol. 103, No. ST6, Proc. Paper 12982, June 1977, pp. 1189–1205.
- [8] Report of the Committee on Inquiry into the Collapse of the Cooling Tower at Ferrybridge, Monday, November 1, 1965, Central Electricity Generating Board, Her Majesty's Stationary Office, London, 1966.
- [9] Gardner, N. J., "Response of Cooling Tower to Turbulent Wind," *Journal of the Structural Division*, Proc. of the American Society of Civil Engineers (ASCE), Vol. 95, No. ST10, Oct. 1969, pp. 2057–2075.
- [10] Kapania, R. K., and Yang, T. Y., "Time Domain Random Wind Response of Cooling Towers," *Journal of Engineering Mechanics*, Vol. 110, No. 10, Oct. 1984, pp. 1524–1543.
- [11] Shiau, L. C., and Yang, T. Y., "Two-Cylinder Model for Wind Vortex-Induced Vibration," *Journal of Engineering Mechanics*, Vol. 113, No. 5, May 1987, pp. 780–789.
- [12] Gero, D., *Military Aviation Disasters*, Patrick Stephens, London, 1999.
- [13] Baz, A., Poh, S., and Fedor, J., "Independent Modal Space Control with Positive Position Feedback," *Journal of Dynamic Systems, Measurement, and Control*, Vol. 114, No. 1, March 1992, pp. 96–103.
- [14] Liu, Y. C., and Yang, S. M., "Three Simple and Efficient Methods for Vibration Control of Slewing Flexible Structures," *Journal of Dynamic Systems, Measurement, and Control*, Vol. 115, No. 4, Dec. 1993, pp. 725–730.
- [15] Devasia, S., Meressi, T., Paden, B., and Bayo, E., "Piezoelectric Actuator Design for Vibration Suppression: Placement and Sizing," *Journal of Guidance, Control, and Dynamics*, Vol. 16, No. 5, 1993.
- [16] Yang, S. M., and Liu, Y. C., "Frequency Domain Control of Flexible Beams with Piezoelectric Actuator," *Journal of Dynamic Systems, Measurement, and Control*, Vol. 117, No. 4, Dec. 1995, pp. 541–546.
- [17] Shen, J. Y., and Sharpe, L., "Finite Element Model for the Aeroelasticity Analysis of Hypersonic Panels, Part 3: Flutter Suppression," *SPIE Proceedings*, Vol. 3039, Paper No. 3039-33, June 1997, pp. 315–323.
- [18] Forster, E. E., and Yang, H. T. Y., "Flutter Control of Wing Boxes Using Piezoelectric Actuators," *Journal of Aircraft*, Vol. 35, No. 6, Nov. 1998, pp. 949–957.
- [19] Olson, M. D., "Finite Elements Applied to Panel Flutter," *AIAA Journal*, Vol. 5, No. 12, 1967, pp. 2267–2270.
- [20] Olson, M. D., "Some Flutter Solutions Using Finite Elements," *AIAA Journal*, Vol. 8, No. 4, 1970, pp. 747–752.
- [21] Yang, T. Y., "Flutter of Flat Finite Element Panels in a Supersonic Potential Flow," *AIAA Journal*, Vol. 13, No. 11, 1975, pp. 1502–1507.
- [22] Yang, T. Y., and Sung, S. H., "Finite Element Panel Flutter in Three-Dimensional Supersonic Unsteady Potential Flow," *AIAA Journal*, Vol. 15, No. 12, Dec. 1977, pp. 1677–1683.
- [23] Han, A. D., and Yang, T. Y., "Nonlinear Panel Flutter Using High-Order Triangular Finite Elements," *AIAA Journal*, Vol. 21, No. 10, Oct. 1983, pp. 1453–1461.
- [24] Afolabi, D., Pidaparti, R. M. V., and Yang, H. T. Y., "Flutter Prediction Using an Eigenvector Orientation Approach," *AIAA Journal*, Vol. 36, No. 1, 1998, pp. 69–74.
- [25] Hanagud, H., Obal, M. W., and Calise, A. J., "Optimal Vibration Control by the Use of Piezoceramic Sensors and Actuators," *Journal of Guidance, Control, and Dynamics*, Vol. 15, No. 5, Sept.–Oct. 1992, pp. 1199–1206.
- [26] Banks, H. T., Smith, R. C., and Wang, Y., "Modeling of Piezoceramic Patch Interactions with Shells, Plates, and Beams," *Quarterly of Applied Mathematics*, Vol. 53, No. 2, 1995, pp. 353–381.
- [27] IEEE Standard on Piezoelectricity, American National Standards Inst./Inst. of Electrical and Electronics Engineers Standard 176-1987, New York, 1988.

- [28] Moon, S. H., and Kim, S. J., "Active and PassiveSuppressions of Nonlinear Panel Flutter Using Finite Element Method," *AIAA Journal*, Vol. 39, No. 11, Nov. 2001, pp. 2042–2050.
- [29] Moon, S. H., Chwa, D., and Kim, S. J., "Feedback Linearization Control for Panel Flutter Suppression with Piezoelectric Actuators," *AIAA Journal*, Vol. 43, No. 9, 2005, pp. 2069–2073.
- [30] Friedland, B., *Control System Design*, McGraw–Hill, New York, 1986, pp. 337–350.

S. Saigal
Associate Editor